AIAA Atmospheric Flight Mechanics Conference
08 - 11 August 2011, Portland, Oregon

AIAA 2011-6527

Experiments on Free-to-Pivot Hover Motions of Multi-hinged Flat Plates

Kenneth Granlund[1] and Michael OL[2]
U.S. Air Force Research Laboratory, Wright-Patterson Air Force Base, OH 45433, U.S.A.

Luis Bernal[3]
University of Michigan, Ann Arbor, MI 48105

Abstract

We extend recent work on flat plates undergoing imposed translation of their leading edge, hinged at the leading edge and free to pivot between 45° angle limiters, to several parameter studies. The first considers aspect ratio effects, with the finding that aspect ratio affects flowfield history but not aerodynamic force history (thrust production or resistive force). The second considers various duty cycles of imposed leading edge acceleration, with the finding that there is not a discernable acceleration effect on aerodynamic force history, and in particular no memory-effects after the plate has attained its limiting incidence angle. The third study compares single-element plates hinged at the leading edge, with double element plates, the latter having a second hinge running spanwise along the midchord. The latter is a surrogate for preliminary study of structural flexibility effects. Double-element plates produce both less thrust and have less resistive force, resulting in most cases in slightly lower figure of merit than that of comparable single-element plates, except for very small stroke to chord ratios.

Nomenclature

θ	Plate pitch angle perpendicular to translation
b	Plate span
c	Plate chord (=50mm)
h_0	Nondimensional translation amplitude $=h/c$
A_s	Swept area $=2bh_0c$
C_N	Coefficient of normal force in direction of translation $=N/(0.5U^2_{ref}bc)$
C_T	Coefficient of thrust perpendicular to direction of translation $=T/(0.5U^2_{ref}bc)$
M	'Figure of Merit' fraction of ideal-to-actual thrust power
U_{ref}	Maximum translation velocity

Introduction

A significant challenge for flapping-wing Micro Air Vehicles, especially in hover, is to achieve flight control authority through modulation of flapping wing kinematics, without relying on a conventional fixed-wing empennage. Considerations of weight and mechanical complexity generally mean minimizing the actuated degrees of freedom by relying on passive deflections to orient the flight surfaces in aerodynamically favorable positions. Doman et al.[1] proposed a flight control scheme for the flapping-wing configuration developed by Wood et al.[2], where the wing leading edge is directly actuated in a sweeping motion, but the wing incidence angle is free to float between limiters. The incidence angle is generally right at the limiter throughout the "translation" phase of each half-stroke, with a rapid rotation from one limiter side to the other, at or near the extrema of each half-stroke. Doman et al[1] assume a quasi-steady lift coefficient time history throughout the translation stroke, using the lift and drag relations developed by Dickson et al.[3], and a non-lifting rotation phase. The former assumption is probably justified for conceptual-design purposes based on results for sinusoidal periodic plunge (Ol et al.[10]), where one finds remarkable robustness of the simple $C_L = 2\pi\alpha$ even for large incidence angles, whether or not a leading edge vortex is present. But the latter assumption is only valid if the stroke fraction occupied by the rotation is small, and post-rotation transients dye out quickly. And since the incidence angle time history during rotation is passively accepted from the combination of body dynamics (wing mass and moment of inertia, hinge dynamics, etc.) and aerodynamic loads (time history of pressure distribution on the wing), the actual incidence angle history is not known a priori. In a previous study by Granlund et al.[4], both thrust- and normal coefficient were found to be independent of Reynolds number (translation velocity or oscillation frequency)and aspect ratio, obtaining essentially the same force history for a

[1] Post-Doctoral Scholar, Air Vehicles Directorate, Kenneth.Granlund@wpafb.af.mil
[2] Senior Aerospace Engineer, Air Vehicles Directorate, Michael.Ol@wpafb.af.mil
[3] Associate Professor, Department of Aerospace Engineering, lpb@umich.edu

nominally 2D and aspect ratio 3.4 plate. Here we extend previous study[4] by considering an intermediate aspect ratio of 5.5.

Several authors[5,6,7] have documented the importance of the leading edge vortex (LEV) in aerodynamic force production, both in translational and rotational motion. Jones and Babinsky[8] offer the suggestion that acceleration of the plate leading edge may promote LEV stability, and inversely, a sharp acceleration of the leading edge followed by a long run of steady translational speed may lead to early LEV ejection. In an attempt to investigate this conjecture, we compare a "trapezoidal" version of the sinusoidal plate leading edge translation, thereby varying the duty cycle of acceleration of the leading edge, at Reynolds numbers from 5,000 to 20,000 based on leading edge maximum velocity.

Flight-article flapping wings are expected to be flexible. As an initial attempt to study aeroelastic effects in the lumped-parameter sense, we introduce a second passive degree of freedom by splitting spanwise the plate hinged at its leading edge, into a pair of plates. The new plate has a moment-free ±45° hinge at its midchord, effectively creating a two-element chordwise discrete aeroelastic wing. The two-element plate is inspired by the idea of Eldredge et al[13]. Such a case has also been computed by Wan et al.[9] for different chordwise hinge locations, but only for one mass property. For small amplitude, high frequency oscillations, the mass of the plate is believed to have an effect on kinematics, and we therefore use plates of different thickness for the same planform, to vary the plate mass. More properly, this varies the ratio of plate effective "density" to that of the ambient fluid.

The overall question is to what extent intra-cycle velocity and acceleration history of flapping wings in hover affects the aerodynamic force generation, how such force production correlates with LEV formation and stability, and how these phenomena may be modified by introducing lumped-parameter aeroelastic effects.

Experimental Setup

Facility and Motion Mechanism

The U.S. Air Force Research Laboratory's (AFRL) Horizontal Free-surface Water Tunnel is fitted with a three degree of freedom electric rig enabling independent control of pitch or rotation, plunge or heave, and "surge" or streamwise-aligned translation. In the present study, the tunnel is operated as a towing tank, with the rig providing the model motions. Nonzero free-stream can be added as surrogate for gust response. A photograph of the tunnel and two model installations are shown in Figure 1. More detail on the rig operation and discussion of experimental error are given in Ol et al.[10], while the facility is discussed in Ol et al.[11]

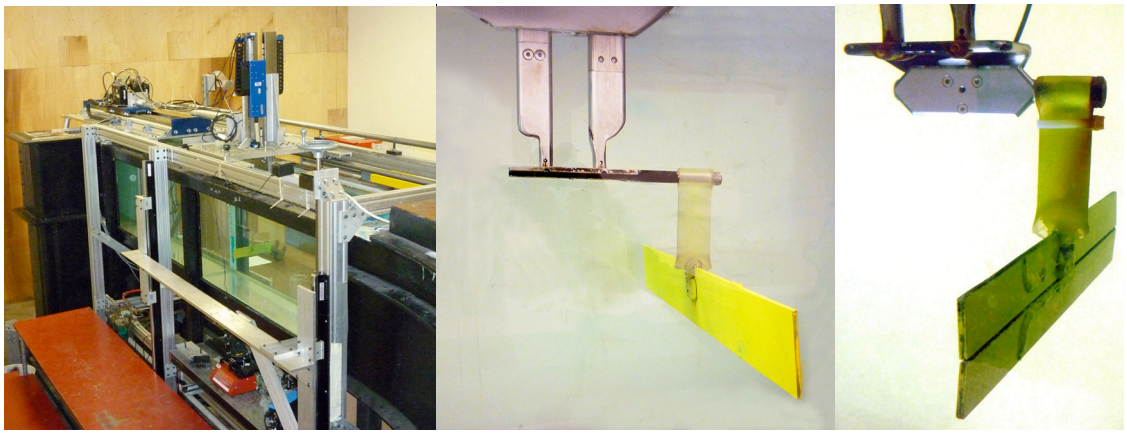

Figure 1. Test section and motion apparatus mounted above test section of the AFRL Horizontal Free-surface Water Tunnel (left); wall-to-wall single-hinge plate set up for sinusoidal imposed fore-aft translation (middle) and AR=5.5 dual-hinge plate (right). The force balance is located behind the metal bracket in the right-hand image.

The motion rig is controlled through a Galil DMC 4040 Ethernet controller. Pitch and plunge are via a pair of motors mounted vertically on a plate above the tunnel test section, shown in the middle

portion of Figure 1. Each motor actuates a vertical "plunge rod", which connects via a bushing to a coupler piece. In prior work[12], the coupler piece was imbedded in an airfoil or flat-plate model. This is acceptable for runs with nonzero free stream, where presumably interference from the plunge rods would result in separated flow structures convecting downstream. But with the water tunnel run as a tank, there is no convective relief from interferences, and therefore to better isolate the model from the rig, a cantilever mounting arrangement is used, depicted in the middle portion of Figure 1. For imposed-translation experiments, a nominally 2D plate is wall-to-wall with 1.0 mm gap on each tip, 5 cm chord, 6% thickness and rectangular edges. AR=5.5 and 3.4 plates have spans of 28cm and 17cm respectively, and are identically mounted and oscillated. The double-hinged plate in the right portion of Figure 1 has a sandwiched nylon cloth sheet as a moment free hinge. The test section floor is ~6 chords below the plate trailing edge and the free surface is ~5 chords above the plate leading edge.

In the present experiment, the two vertical motors of the motion rig are used only to pre-position the model at maximum elevation above the tunnel test section floor, to reduce ground-effect. Imposed fore-aft motion of the plate's leading edge is via the horizontal or "surge" linear motor.

In free-to-pivot imposed translations, the model is hinged at the midspan of its leading edge, and constrained to rotate within ±45° from its rest (vertical) position. As its support is translated, pressure difference between the advancing and retreating side forces the plate against one of its pitch limiters, effectively placing it at 45° angle of attack. This is reversed in the opposite direction of translation.

Force Measurement and Flow Visualization

For dye injection, stainless steel lines with 0.5mm internal diameter, injecting concentrated blue food coloring, were glued to the model surface at the ¾ span location at the leading and trailing edge, firing away from each respective edge in the chord plane. Milk is used to reduce diffusion and ethyl alcohol is added to bring density of dye mixture closer to that of the ambient water. Unfortunately, for hover experiments dye injection is less successful than for motions with free-stream[10], because large strain rates cause rapid dye dissipation, while running the dye at high flow rates introduces unacceptable disturbances of the ambient flow and large agglomerations of dye near the motion stroke endpoints.

Force measurements were with an ATI Nano-25 IP68 6-component balance. For maximal force balance sensitivity and reduction of vibrations, the balance should be near the model's center of pressure. This however introduces rather unacceptable interference. A cleaner arrangement is a strut mount with the leading edge hinge located some distance away from the balance, and the balance is integrated into a housing that connects to the two vertical plunge rods. Here one must be careful about the stiffness of the strut and the balance itself. The loadcell is very stiff in force load, but less so in torque. Since the forces on the loadcell are generally understood to be in the translation direction orientation, one must not place the model too far below the loadcell, to reduce the moment arm.

Results

We discuss the collection of test cases, then consider flow visualization results, then force histories, and finally assess propulsive efficiency.

Test matrices for the various case studies are as follows: Table 1 compares the 2D, AR=5.5 and AR=3.4 single-element plates undergoing leading-edge sinusoidal motion; Table 2 compares sinusoidal and trapezoidal LE motion profiles for the AR=5.5 single element plate; and finally, Table 3 compares the single-element plate, with two kinds of double-element plates: standard mass (standard thickness) and lightened mass (halved thickness), all for AR=5.5 and sinusoidal imposed motion.

Table 1. Aspect ratio study (2D, AR=3.4 and AR=5.5), single-element plate, sinusoidal LE motion. Semi-stroke to chord ratio in columns, and physical frequency of LE motion (Hz) in rows. Nominal Reynolds number (left column) is proportional to product of frequency and semi- stroke. Every entry represents a run for each of the three plates.

Frequency	Semi-stroke to chord ratio				
Nominal Re	6.20	3.10	1.55	0.775	0.3875
6,500	0.1055	0.211	0.422	0.844	1.688
8,300					2.128
13,000	0.211	0.422	0.844	1.688	

16,400		0.532	1.064		
21,900	0.355				

Table 2. Motion profile study, single-element AR=5.5 plate, comparison of sinusoidal imposed LE motion, a = 2 and a = 3.

Frequency	Semi-stroke to chord ratio			
Nominal Re	3.10	1.55		
6,500	0.211	0.422		
13,000	0.422	0.844		

Table 3. Study of single vs. double-element plates of (a) standard mass and (b) lightened mass; AR = 5.5, sinusoidal LE imposed motion profile. Every entry represents a run for each of three plates: single-element AR=5.5, standard-mass AR=5.5, and lightened-mass AR=5.5.

Frequency	Semi-stroke to chord ratio			
Nominal Re	3.10	1.55	0.775	0.3875
6,500	0.211	0.422	0.844	1.688
8,300				2.128
9,700				2.532
13,000	0.422	0.844	1.688	
16,400	0.532	1.064		

The prescription of LE representative kinematics is given in Figure 2. Difference between prescribed and attained LE motion was shown to be negligible in Granlund et al.[4] Figure 2 compares four families of LE motion: purely sinusoidal ("cos"), and several "trapezoidal" motions, where the LE translation speed is a smooth linear ramp, followed by a constant-velocity run before smoothed linear deceleration at the opposite end of the semi-stroke. Smoothing is based on a C^{∞} function developed by Eldredge et al. [13], here written in terms of fore-aft motion parameters (eqn. 1).

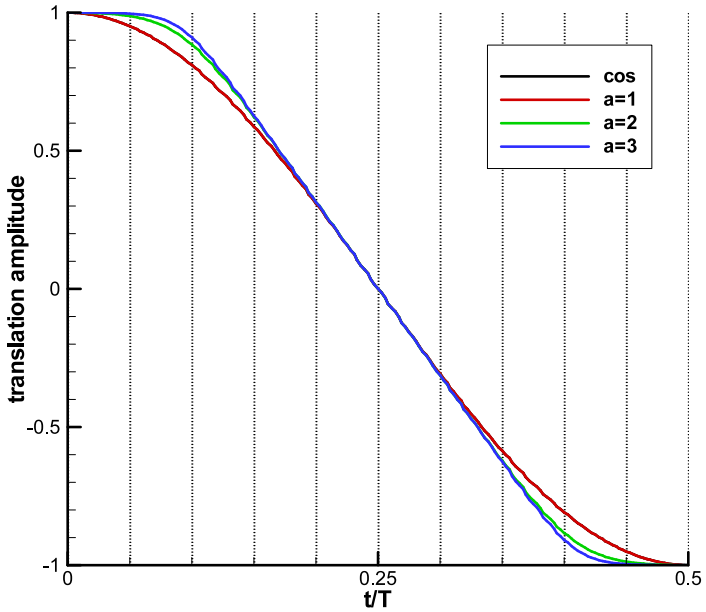

Figure 2. Nondimensional sinusoidal and trapezoidal translation motion profiles. Sinusoidal is coincident with a = 1. One semi-stroke is shown.

$$\frac{amplitude}{\max(amplitude)} = -1 + 2\ln\left(\frac{\cosh\left(a\left(t/T - \frac{\pi-2}{4\pi f}\right)\right)\cosh\left(a\left(t/T - \frac{3\pi-2}{4\pi f}\right)\right)}{\cosh\left(a\left(t/T - \frac{\pi+2}{4\pi f}\right)\right)\cosh\left(a\left(t/T - \frac{3\pi+2}{4\pi f}\right)\right)}\right) \qquad (1)$$

The parameter "*a*", which controls the amount of smoothing (Figure 2), is a dimensionless acceleration upper bound. The case of *a*=1 is indistinguishably close to the sinusoid, whence we consider the three cases of sinusoid, *a*=2 and *a*=3. The upper bound of "*a*" is limited by rig acceleration in periodic motion of the relatively heavy horizontal carriage (that is, overheating of the linear motors).

Representative measurements of the plate incidence angle history, as extracted from flow visualization video, are given in Figure 3, for the AR=5.5 single-element plate. The plate is indeed seen to pivot between ±45º limits, but with up to 2º overshoot, due to slop in the hinge mechanism and elastic compliance in the hinge housing. If there were zero phase lag between the translation and rotation, the plate would be hanging vertically at translation phases of 0 and 180 degrees. Instead, the rotation lags the translation, akin to the "delayed rotation" variant of normal-hover[14]. The longer the translation stroke to chord ratio, the lower the phase lag in rotation becomes.

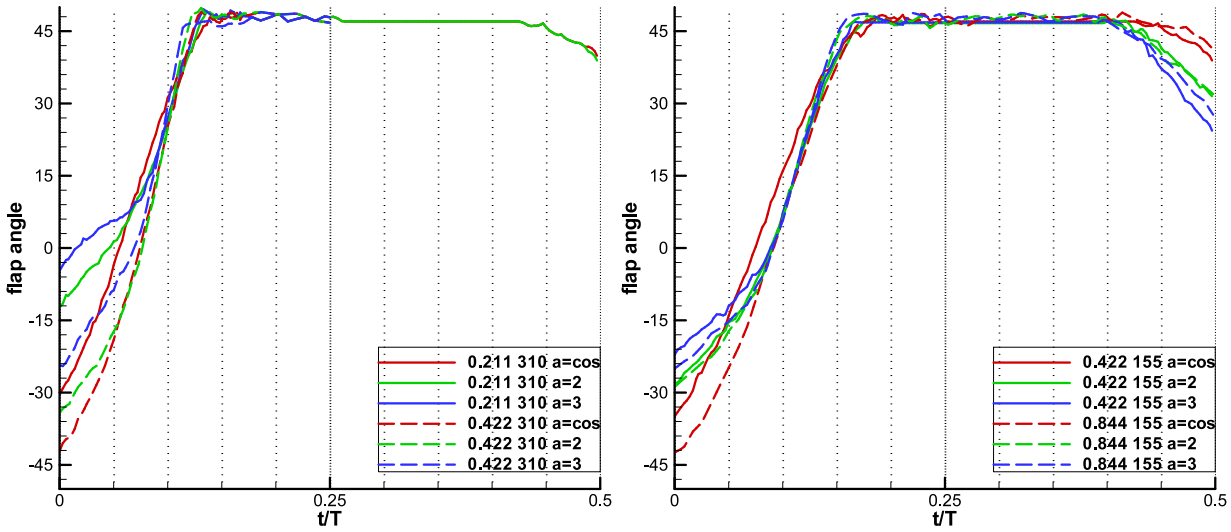

Figure 3. Measured history (from video) of AR=5.5 single-element plate incidence angle for 3.1c (left) and 1.55c (right) semi-stroke for two frequencies and three translation motion profiles; only one semi-stroke shown.

To within ±0.03t/T, the plate reaches its angle limiter at the same phase of translational motion, regardless of whether the acceleration profile is sinusoidal or trapezoidal. This means that the portion of the motion history where the plate is at 45° incidence, begins essentially at the same time for all cases.

Flow visualization in translation motion of wall-to-wall plate

We first consider a survey of reduced frequency/amplitude, keeping Reynolds number constant. In the absence of an imposed free-stream, reduced frequency becomes a purely kinematic variable, and is here is taken as the ratio of stoke amplitude to plate chord. Figure 4 shows snapshots of dye injection for every 30 degrees of phase of fore-aft sinusoidal motion of the plate leading edge, for three cases, all for AR=5.5 plates, and all with a Reynolds number of 13,000: single-element plate at 0.844Hz and 1.55 chord amplitude; double-element standard-mass plate at 0.844Hz and 1.55 chord amplitude, and double-element standard-mass plate 1.688Hz and 0.775 chord amplitude. Phase "0" refers to the right extremum of the leading-edge fore-aft motion.

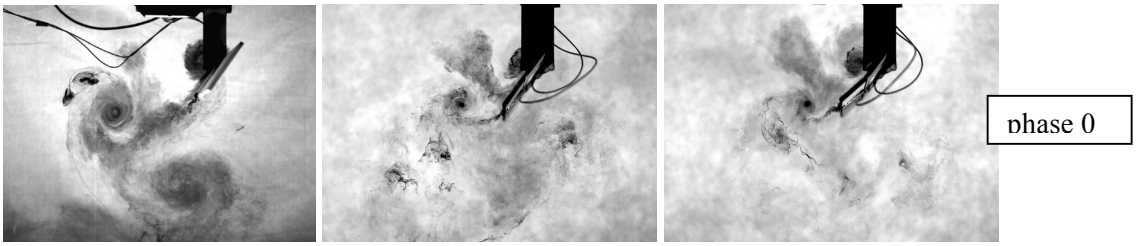

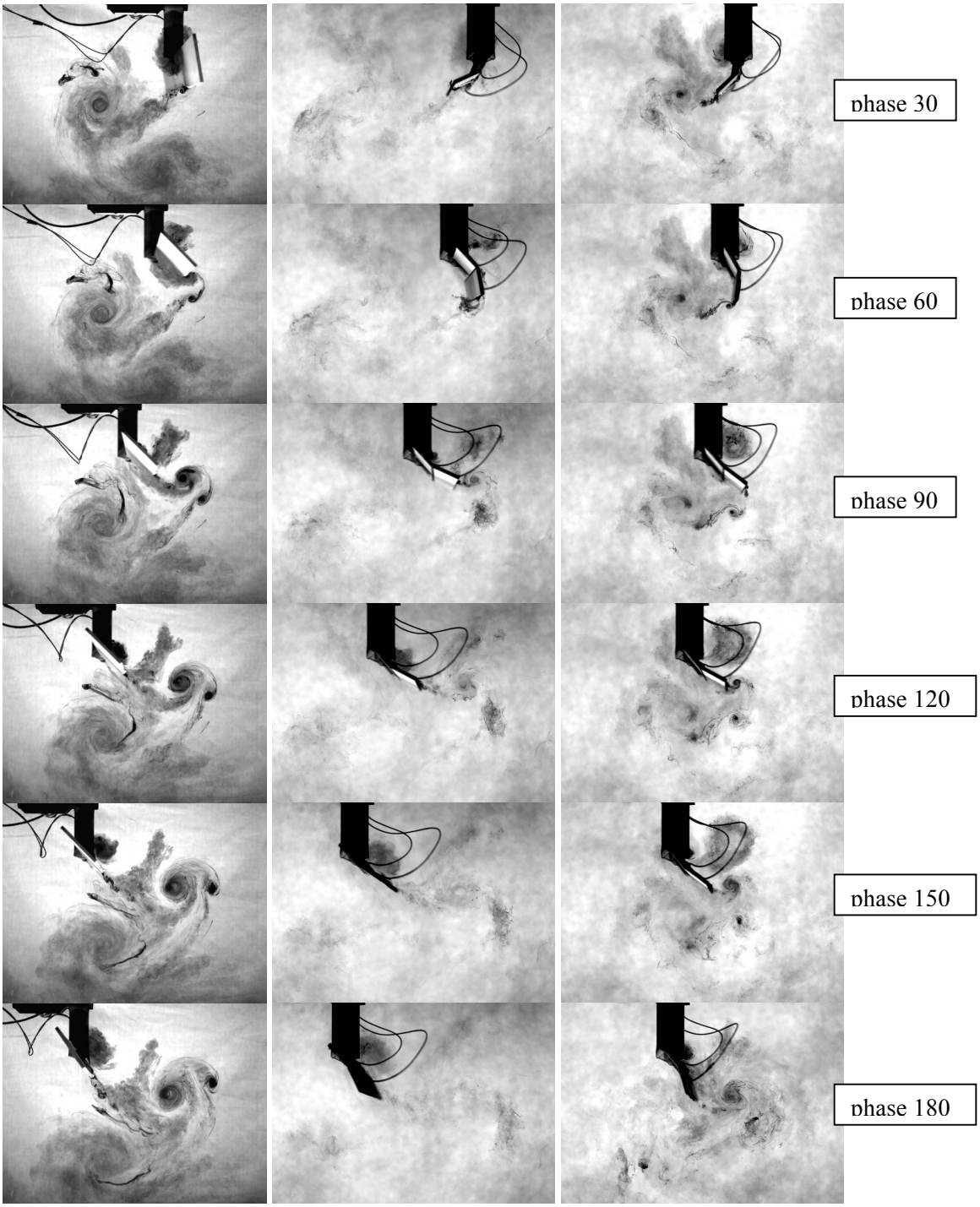

Figure 4. Dye injection snapshots for three sinusoidal fore-aft traverses for AR=5.5 plates: 0.844 Hz, 1.55c amplitude single-element (left column); 0.844 Hz, 1.55c amplitude double-element (2nd column); 1.688Hz, 0.775c amplitude double-element (right column). From top to bottom, with phase 0 = right-most extreme of translation stroke, snapshots are at phase = 0, 30, 60, 90, 120, 150 and 180 degrees. Nominal Re = 13,000.

Figure 5 compares the flowfield for three more sinusoidal motions of the AR=5.5 plate, all with a Reynolds number of 6,500 and oscillation at 0.422Hz with 1.55 chord amplitude. The leftmost case is with a single-element plate, the middle with a double-element plate and the rightmost also with a freestream velocity from left to right at half the maximum translation velocity.

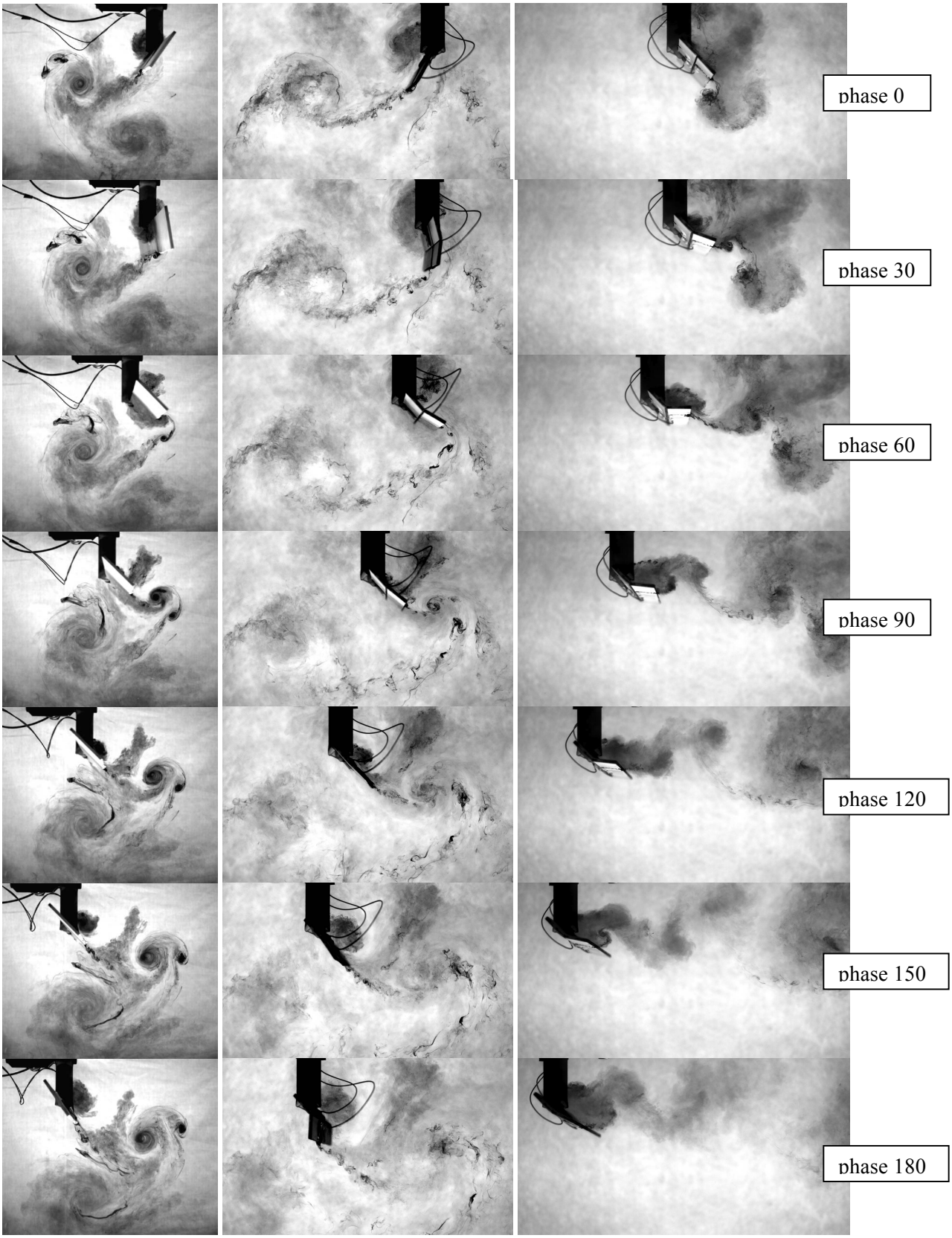

Figure 5. Dye injection snapshots for three sinusoidal fore-aft motions of AR=5.5 plates at 0.422 Hz frequency, 1.55c amplitude: single element (left column); double element (2nd column); double element with horizontal velocity from left to right (right column). In going from top to bottom, with phase 0 = right-most extreme of translation stroke, snapshots are at phase = 0, 30, 60, 90, 120, 150 and 180 degrees. Nominal Re = 6,500

A strong trailing edge vortex forms shortly after translation stroke reversal, but is quickly shed.

This is common to all cases. Beyond that, the flowfield evolution varies case by case. For the case with a normal freestream velocity, a recirculating region forms on the lee side of the plate. Presently with dye visualization there is insufficient information to regard this as an LEV or not; but in any case, the entire lee side of the plate is covered by a concentration of dye convecting together with the plate, for approximately half of the translation semi-stroke. The main conclusion from these results is the comparatively higher diffusivity of dye-visualized vortices, at least for the larger semi-stroke to chord ratios, for the AR=5.5 plate vs. that of the 2D plate (for the latter, see Granlund et al.[4]). We next consider whether flowfield-differences for different aspect ratios result in differences in aerodynamic force history.

Force measurements on single-element plates of various aspect ratio

Thrust is taken to be in the vertical direction in the lab reference frame; that is, normal to the direction of leading edge fore-aft translation. Normal force is in the direction opposing the fore-aft translation. Thus, "thrust" is a kind of lift, while "normal force" becomes a drag.

Figure 6 surveys thrust and normal force coefficients for a range of translation amplitudes for the three different aspect ratio single-element plates with sinusoidal LE motion. Coefficients are obtained from normalization with respect to the peak fore/aft LE translation speed for each respective case.

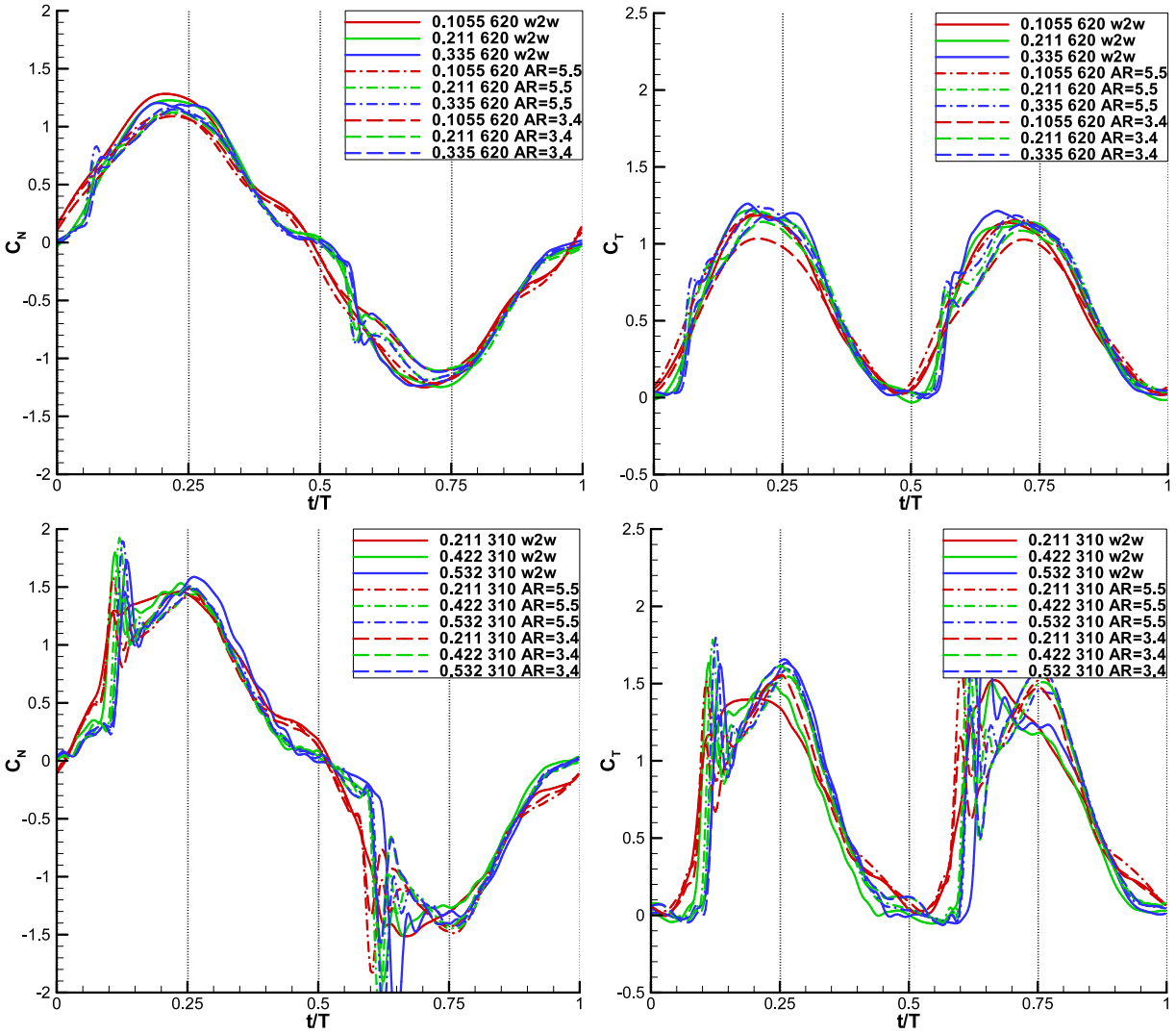

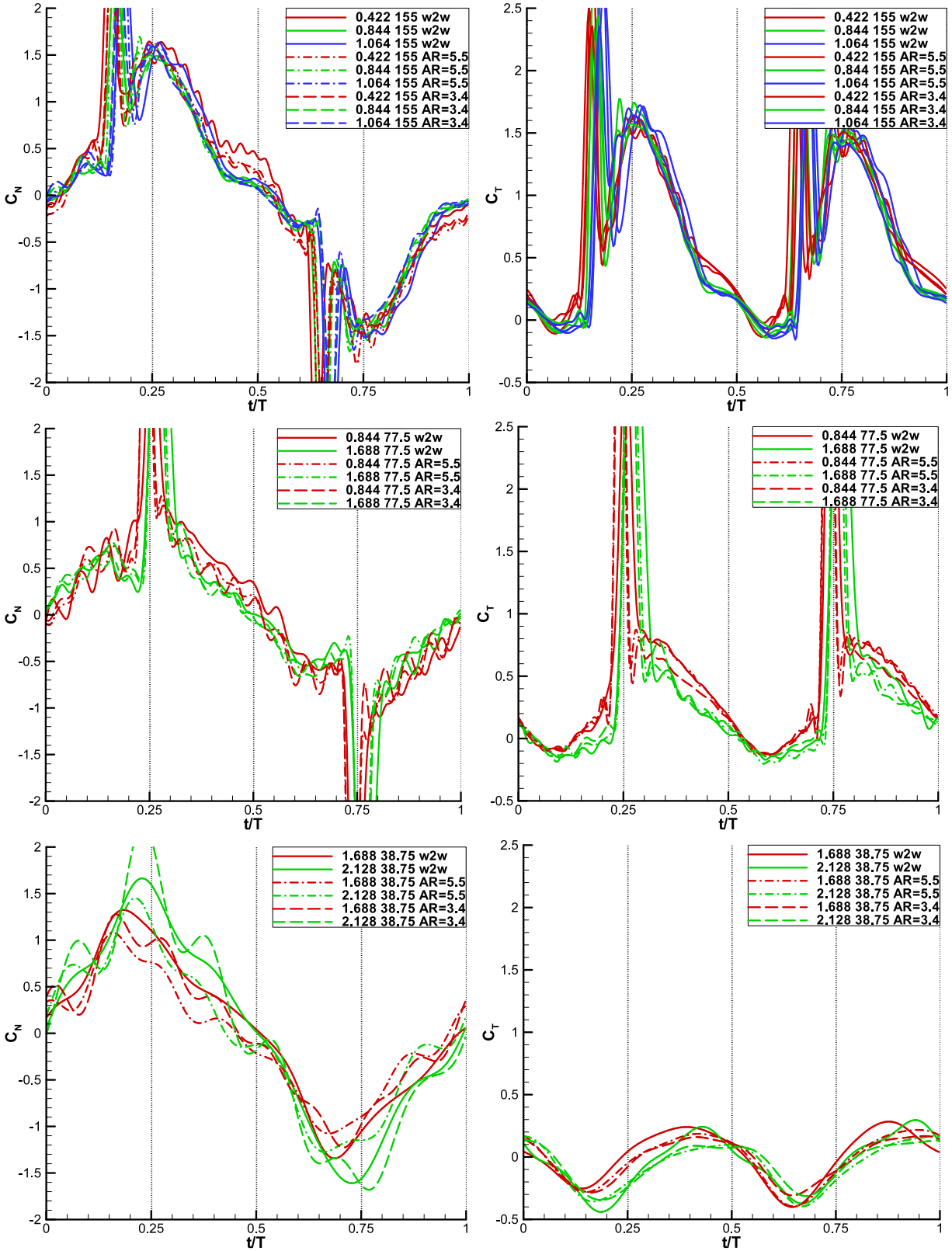

Figure 6. Normal force coefficient (left column) and thrust coefficient (right column) for various frequencies of sinusoidal oscillation of single-element 2D plates. Coefficients are based on maximum translation velocity. Reading from top to bottom row, semi-stroke amplitudes are 6.2c, 3.1c, 1.55c, 0.775c and 0.3875c.

Each row of Figure 6 compares the three plates at different frequencies, while holding semi-stroke to chord ratio constant. In turn, each row of Figure 6 covers a different semi-stroke to chord ratio, from highest (6.2, top row) to lowest (0.3875, bottom row). This amounts to a Reynolds number survey and an aspect ratio survey within in each row of Figure 6.

The various curves in each respective row in Figure 6 nearly overlap, implying the lack of a discernable trend either with respect to Reynolds number or plate aspect ratio, in either thrust or normal force. Of course, if the fore-aft speed is so low that the plate has insufficient momentum to swing fully from pitch limiter to pitch limiter, its kinematics history will be an outlier, producing a fictitious Reynolds number effect. This happens for example for the 0.211 Hz, 3.1c case. Excluding that exigency, we conjecture that Reynolds number is unimportant in affecting thrust or normal-force production, because separation occurs from high adverse pressure gradients – that is, at the plate's edges, and due to large incidence angle excursions. We do not have a viable conjecture for why aspect ratio would be so unimportant to thrust or normal-force history. But it is striking that aspect ratio matters considerably more for flowfield history than for force history.

One can also observe from Figure 6 that a force 'spike' occurs near t/T=0.125 for the 3.1c amplitude case, and progressively later in phase for decreasing amplitude. For the 6.1c amplitude case, the physical acceleration of the plate at the translation extremes is apparently not large enough to cause a force 'spike' when it reaches the 45° limiter. For the 0.3875c amplitude at the bottom of Figure 6, the force spike is again attenuated, evidently because the imposed LE translation amplitude is too small to drive the plate against its pitch limiters. Indeed, the plate's motion is essentially a rotation about its midchord, and very little net thrust is produced.

Figure 7 shows an alternative normalization of normal- and thrust-coefficients, using the instantaneous translation velocity of the plate's LE throughout the cycle, instead of the maximum translation velocity.

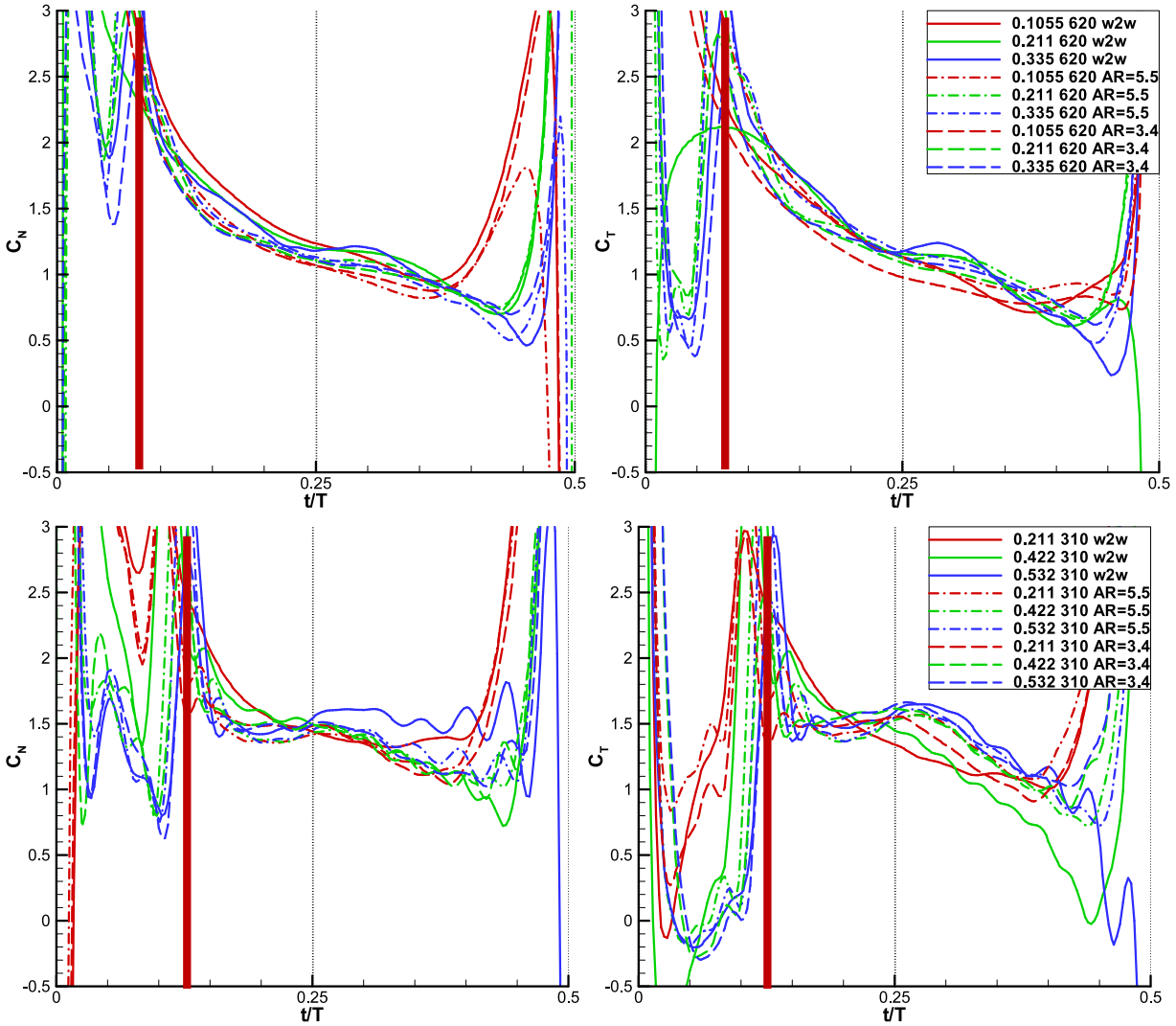

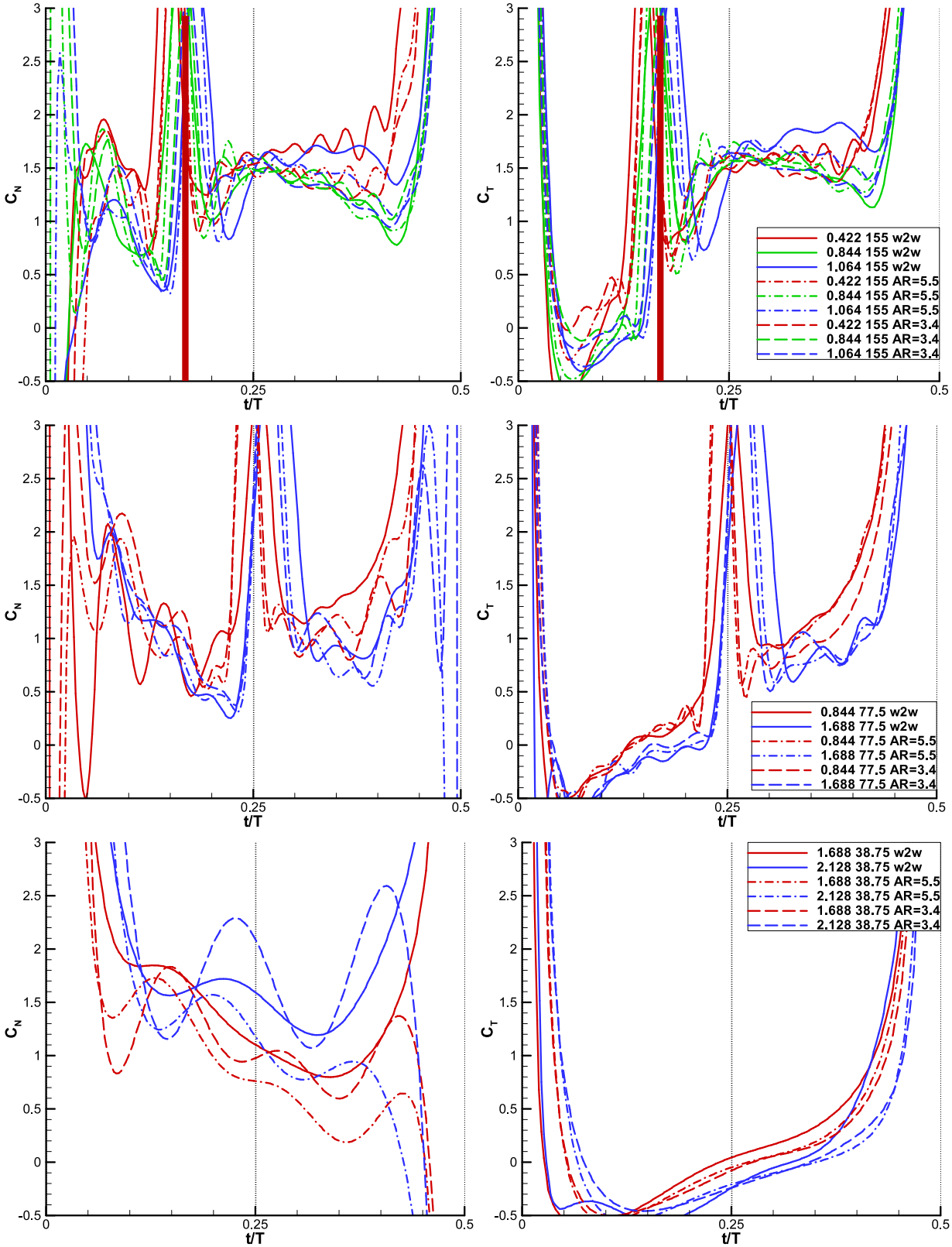

Figure 7. Normal force coefficient (left column) and thrust coefficient (right column) for various frequencies of sinusoidal oscillation of single-element plates. Coefficients based on instantaneous translation speed of the LE. Reading from top to bottom row, semi-stroke amplitudes are 6.2c, 3.1c, 1.55c, 0.775c and 0.3875c. Heavy red vertical line segment represents phase of translation where plate has first attained its incidence limiter, to ±0.03t/T accuracy.

At the translation extrema of *t/T=[0 0.5 1]* where the LE speed is zero, the force coefficients under such normalization will of course approach infinity, and are unreliable in this presentation. But

now trends in force coefficients near the semi-stroke midpoints are easier to observe. Figure 7 includes a marking of the approximate phase of translational motion, where the plate first attains its incidence limiter. This is the beginning of the putative quasi-steady run, since the angle of attack no longer varies between that point and the onset of plate rotation towards the semi-stroke extremum.

If the aerodynamic response were to be truly quasi-steady, then the force coefficient history would have two properties: first, while the plate is rotating from one 45° limiter to the opposing limiter, coefficient history would track incidence history, with no lags or overshoots; and second, once the plate has reached its 45° limiter, and remains thus oriented, the aerodynamic force coefficients should remain constant. These statements are properly true not for the total aerodynamic force history, but only for the circulatory portion. Figure 6 and Figure 7 suggest that the rotation process between limiters is not quasi-steady in any recognizable sense. Plate-limiter impact loads and their smearing in the time-domain due to load-cell data low-pass filtering, together with noncirculatory loads due to acceleration of ambient fluid while the plate rotates, confound interpretation of force coefficient history during the rotation. But force coefficient history during the phase of motion where the plate rests against its limiter is fairly clear in Figure 7. For the 6.2c case, the rotational spike is followed by a more or less linear decay in both thrust coefficient and normal force coefficient from ~1.5 to ~ 1. Such decay is consistent with the findings of Jones and Babinsky[6] for a rotating plate, after the plate has reached a steady rotation speed and the LEV formed during startup-acceleration has shed. For the 3.1c case, the force coefficients behave similarly, with a linear decay, albeit generally with lower slope. For the 1.55c case, however, the force coefficients are more or less constant at a value of ~ 1.5, with no discernable decay. For smaller semi-stroke to chord ratios, interpretation of force history becomes more problematic because the rotational portion of the motion has such a large duty cycle in the overall motion history. But at least for thrust coefficient, it is enticing to ignore the rotational spike and to visualize a linear fit to the thrust coefficient history for $0.1 \leq t/T \leq 0.4$. This results in a positive slope, which is counter-intuitive, and remains to be explained.

With evidence that aspect ratio does not affect thrust or normal-force history, the remainder of the data set (Table 2 and Table 3) is limited to the AR=5.5 plate. Because this plate has more surface area than the AR=3.4 plate, force balance signal to noise ratio is higher. And unlike the 2D plate, there is no danger of the plate's tip striking the test section sidewalls, which is convenient for large parameter studies.

Force measurements on the single-element AR=5.5 plate in various motion profiles

Figure 8 continues the instantaneous LE-speed normalization, for the AR=5.5 single-element plate, in sinusoidal vs. trapezoidal LE motion. Data is limited to 3.1c and 1.55c semi-stroke to chord ratios. For all cases, the force coefficients are very weakly affected by differences in translational acceleration. Differences, such as they are, occur prior to the rotational spike, and as with other such cases, can not presently be segregated between incidence-limiter impacts and noncirculatory effects. We note, therefore, that for the presently-studied range of translational acceleration, the subsequent history of aerodynamic forces is unaffected by acceleration transients.

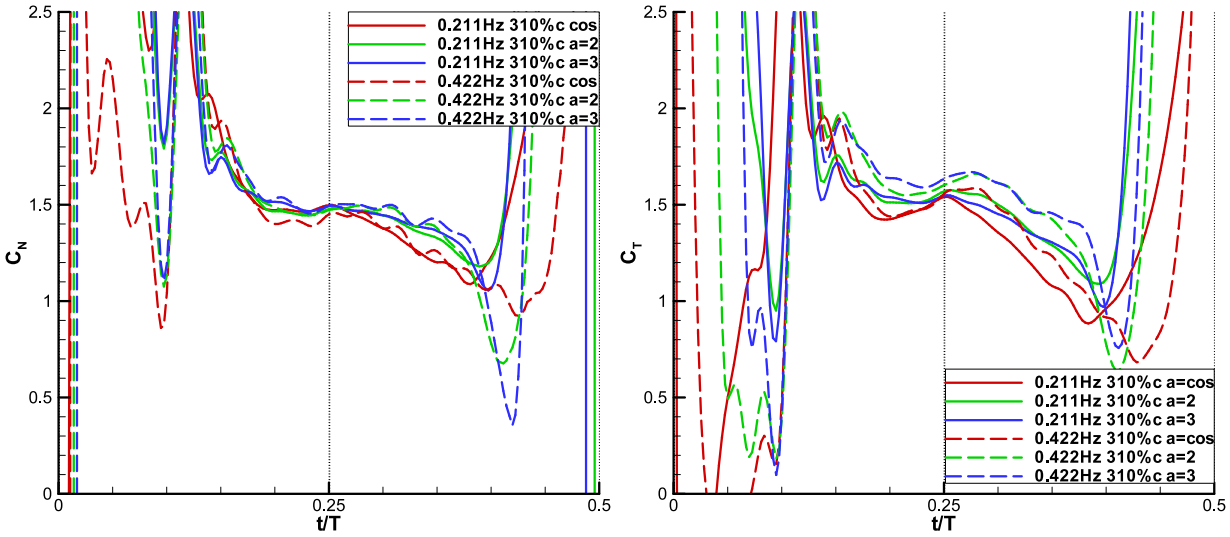

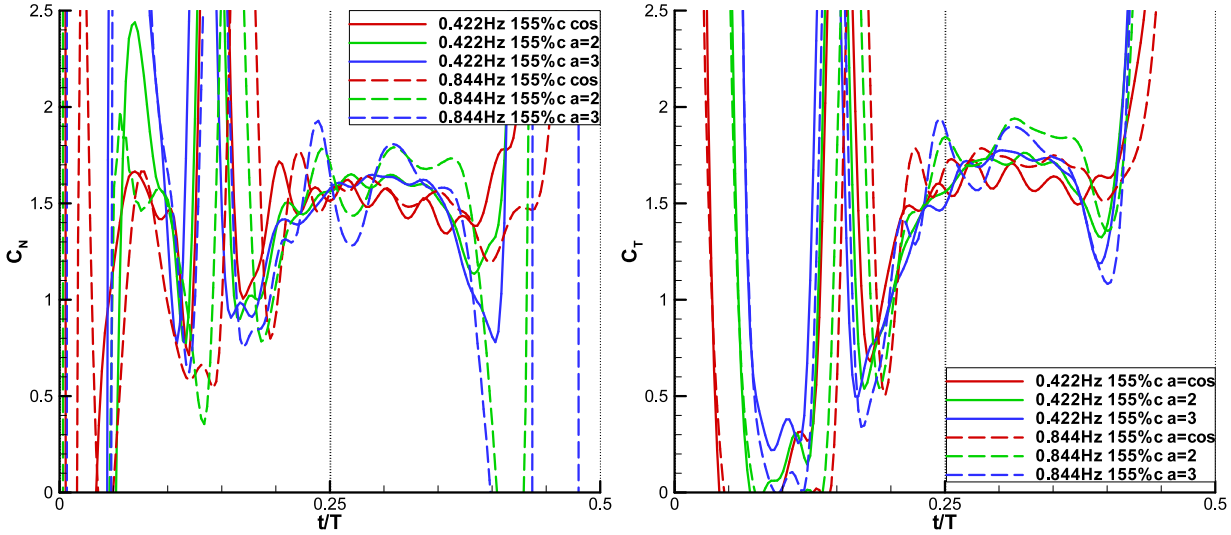

Figure 8. Normal force coefficient (left column) and thrust coefficient (right column) for two frequencies of sinusoidal and trapezoidal motions, AR=5.5 single-element plate. Coefficients are normalized by instantaneous velocity.

Force measurements on single- and double-element flaps

Figure 9 and Figure 10 follow Table 3 in comparing the three AR=5.5 plates: single-element, standard-mass (standard-thickness) double-element, and lightened-mass double-element. The range of semi-stroke to chord ratio is 3.1 to 0.3875. Figure 9 defines coefficients with respect to plate LE peak translational speed, while Figure 10 uses the instantaneous LE translation speed.

The double-hinged plate is seen to have lower thrust- and normal force for the larger motion amplitudes, in particular when the velocity (frequency) is large. As observed in Figure 5, the lower portion of the plate has a reduced angle of incidence compared to the upper portion. This reduces the combined plates' projected area, resulting in smaller forces. But for smaller semi-stroke to chord ratios, the double-hinged plate produces equal, or even larger thrust than the single-hinged plates, despite requiring the same normal force to drive the motion. Evidently, its rotational dynamics are more complicated that the single-element plate's effective rotation about its midchord.

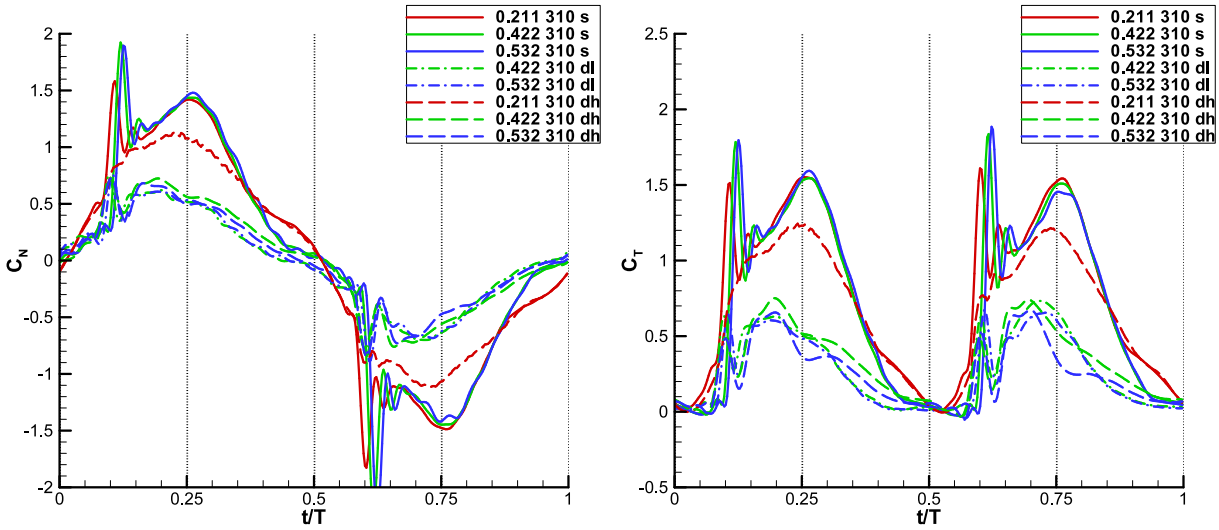

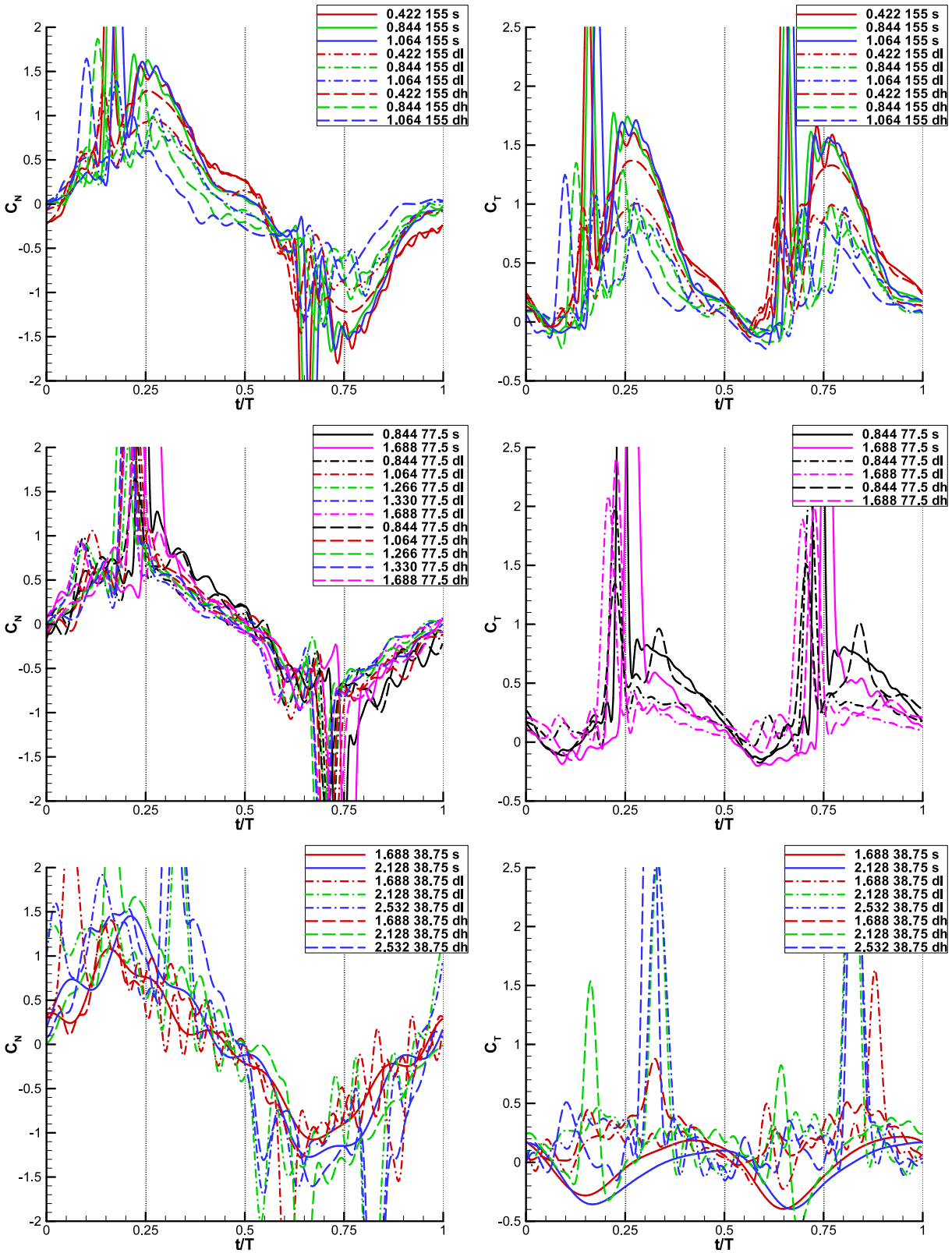

Figure 9. Normal- (left) and thrust (right) coefficient for varying frequency motion of AR=5.5 single element plate (labeled "s"), standard-density double-element plate (labeled "dh"), and lightened-density double element plate (labeled "dl"). Force coefficients normalized by peak LE translation speed. Reading from top to bottom row, leading-edge translation amplitudes are 3.1c, 1.55c, 0.775c and 0.3875c.

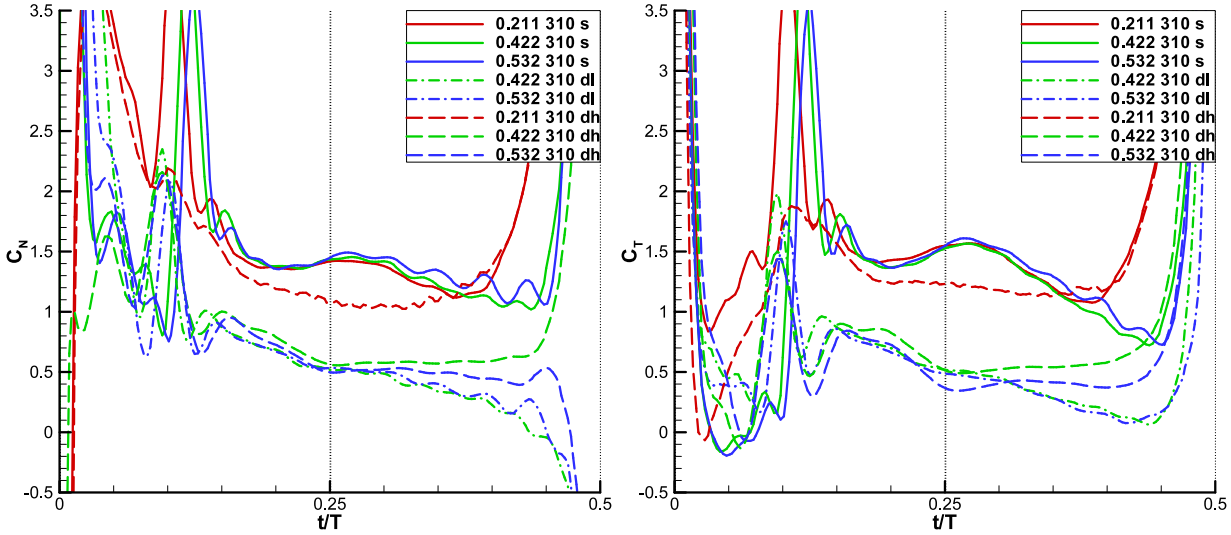
0.211 310 s
0.422 310 s
0.532 310 s
0.422 310 dl
0.532 310 dl
0.211 310 dh
0.422 310 dh
0.532 310 dh
C_N
t/T

0.211 310 s
0.422 310 s
0.532 310 s
0.422 310 dl
0.532 310 dl
0.211 310 dh
0.422 310 dh
0.532 310 dh
C_T
t/T

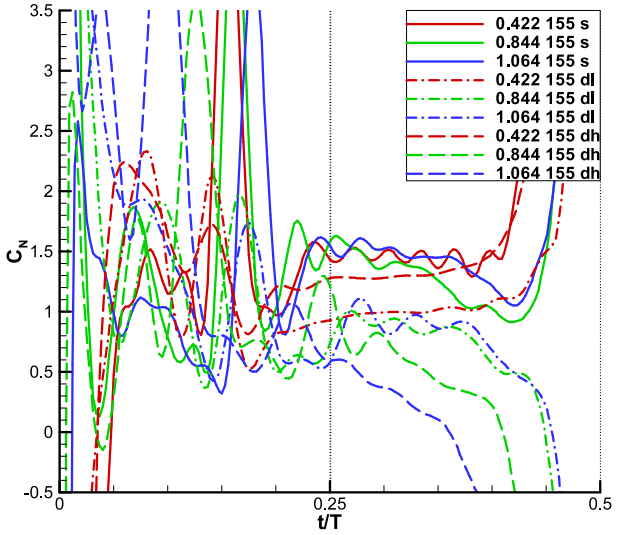
0.422 155 s
0.844 155 s
1.064 155 s
0.422 155 dl
0.844 155 dl
1.064 155 dl
0.422 155 dh
0.844 155 dh
1.064 155 dh
C_N
t/T

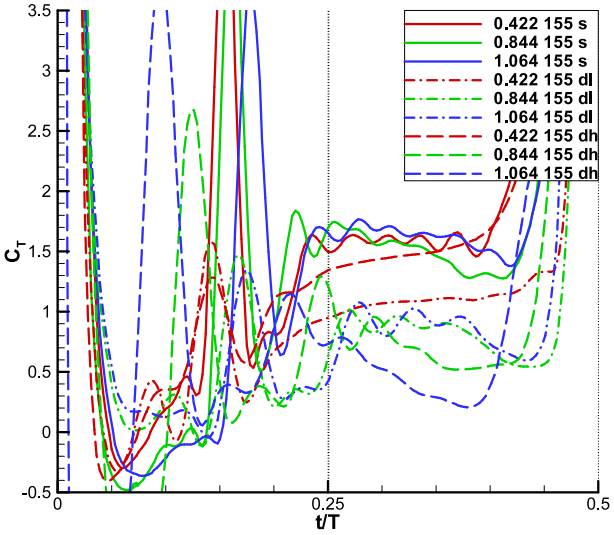
0.422 155 s
0.844 155 s
1.064 155 s
0.422 155 dl
0.844 155 dl
1.064 155 dl
0.422 155 dh
0.844 155 dh
1.064 155 dh
C_T
t/T

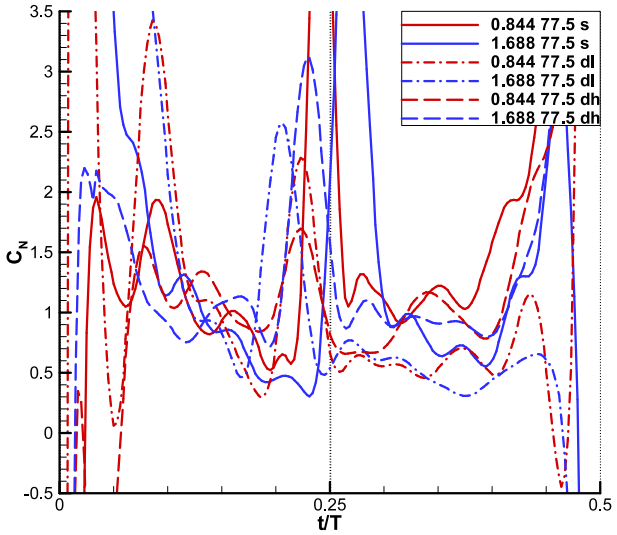
0.844 77.5 s
1.688 77.5 s
0.844 77.5 dl
1.688 77.5 dl
0.844 77.5 dh
1.688 77.5 dh
C_N
t/T

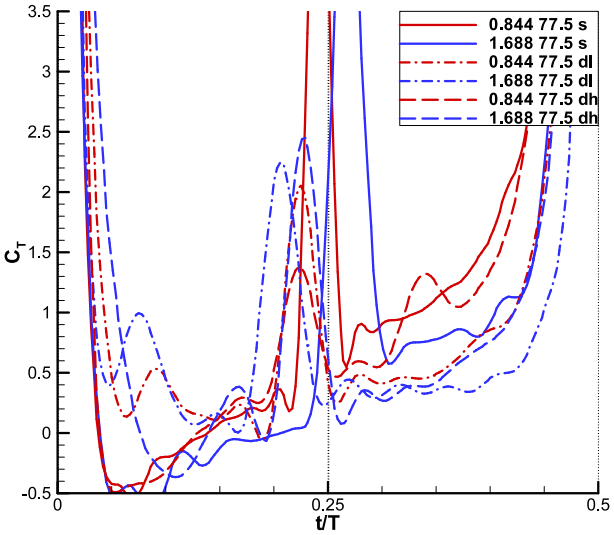
0.844 77.5 s
1.688 77.5 s
0.844 77.5 dl
1.688 77.5 dl
0.844 77.5 dh
1.688 77.5 dh
C_T
t/T

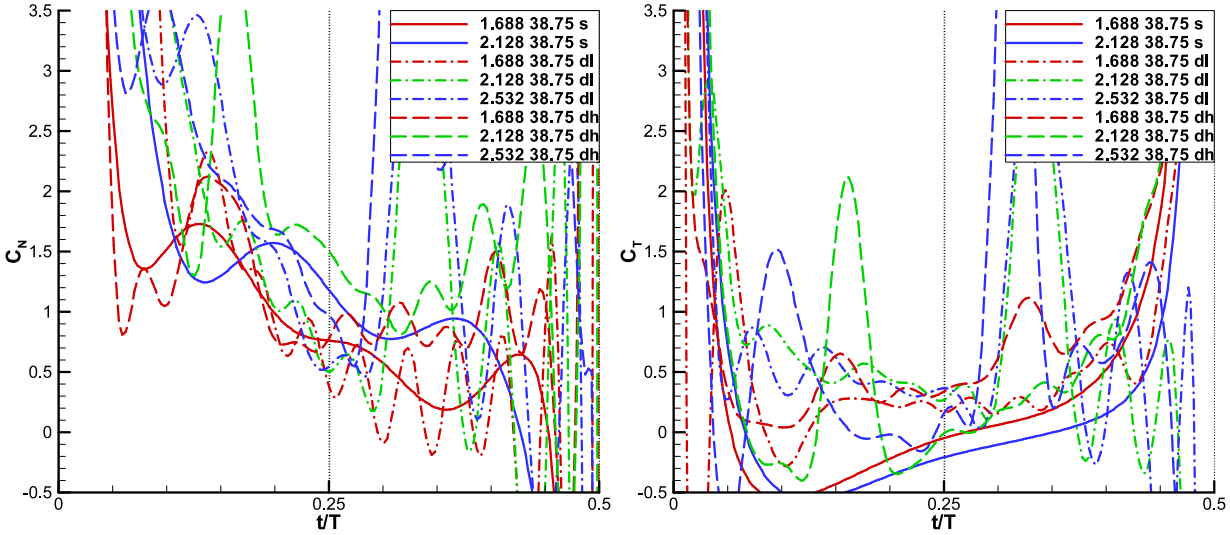

Figure 10. Repetition of Figure 9, with force coefficients normalized by instantaneous LE speed instead of peak LE speed.

For the heavier (thicker) dual-element plate at the lower frequency (slower speed), the dynamic pressure balances the mass*gravity of the trailing element of the plate and causes it to deflect no more than neutral camber with respect to the leading element. During the deceleration phase *0.25<t/T<0.5* the heavier (thicker) heavier trailing element will camber more and maintain thrust at a more constant value than the lighter (thinner) where the normal and thrust coefficients tapers off to zero quicker. The force impulse at *t/T~0.125* is also due to the leading plate hitting the *45°* limiter. The angular acceleration of the trailing plate is apparently not large enough to reach its angle limiter to cause a second spike.

For the smaller 1.55c translation amplitude, higher frequency cases, we can observe double spikes in both normal and thrust direction from first the leading plate and then the trailing plate hitting the limiters except for the lowest frequency for both the double-element flaps. For higher frequencies with the heavier model, the normal force turns negative quicker and maintains lower thrust longer.

For yet smaller amplitude of 0.775c, the double-element models are becoming very similar on both normal- and thrust coefficients as the single element model. For yet another reduction in amplitude to 0.3875c and increase in frequency, the normal force is the same, but now the produced thrust is positive throughout he half-cycle for the double-element model, whereas it is negative for the first quarter- and positive for the second. Because of motion symmetry, a net zero thrust is produced.

Thrust production efficiency

Perhaps the most intuitively cogent scheme for assessing thrust-production efficiency of the various plate motions is the 'figure of merit', *M,* borrowed from helicopter theory (see for example McCormick[15]). *M* is the ratio of ideal power to input power, and is adapted to flapping plates in Equation 3.

$$M = \frac{(C_T)^{3/2}}{2C_P\sqrt{A_s/A_{ref}}} = \frac{(C_T)^{3/2}}{2C_P\sqrt{2h_0 cb/cb}} = \frac{(C_T)^{3/2}}{2C_P\sqrt{2h_0}} \qquad (3)$$

M is plotted for the three types of AR=5.5 plate (single-element, standard-mass double element, and lightened-mass double-element) in Figure 11. For most cases, *M* varies between 0.15 and 0.3. The main outlier is the single-element plate at the smallest semi-stroke to chord ratio, which essentially produces no thrust. Apart from that, there is not a discernable trend in *M* vs. semi-stroke to chord ratio. This may be regarded as favorable news for flapping-wing MAV designers, as the stroke to chord ratio becomes a free variable, lacking an optimal value from an aerodynamic viewpoint. Also, other than for the smallest semi-stroke to chord ratio, the double-element plates have lower *M* than single-element plates, suggesting that at this crude level of regard, flexibility is not beneficial.

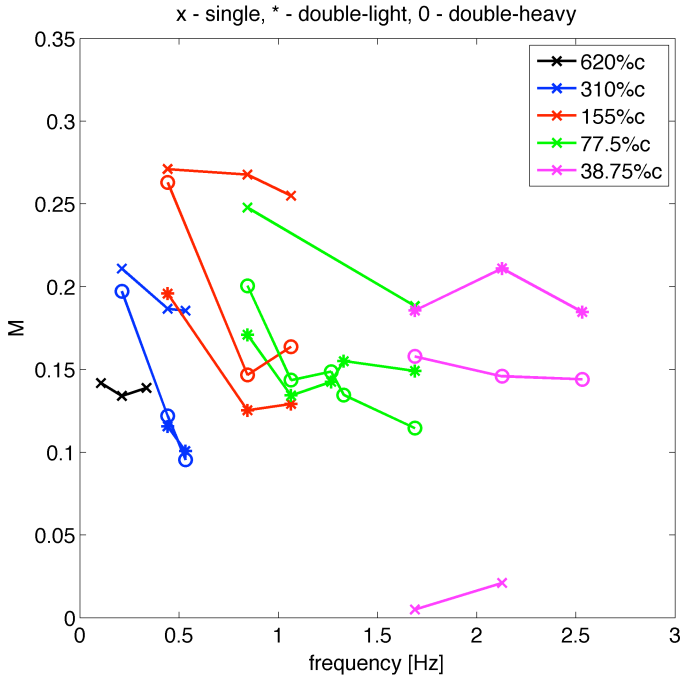

Figure 11. Figure of Merit as a function of translation frequency for AR=5.5 plates (single-element, marked with "x"; double-element with standard mass, marked "0"; and double-element with lightened mass, marked "*").

Conclusion

We consider a parameter study of frequency, amplitude (in combination, Reynolds number), and acceleration profile for free-to-pivot rigid flat plates. Plates have an imposed translation at their leading edge, but pivot within a ±45° range, depending on the dynamics of motion. This is intended as a model for flapping-wing micro air vehicles, were the wing sweeping motion is actuated, but the wing pronation and supination is passive. To begin assessing the role of wing flexibility, at least in a lumped-parameter sense, two kinds of plates are considered: a single-element plate that pivots only about its leading edge, and a double-element plate with its aft half hinged to its forward half.

Formation and history of the leading edge vortex appears to differ between 2D plates and plates of finite aspect ratio (AR=5.5 and 3.4), at least as far as flow visualization by dye injection is able to evince. However, difference in flowfield does not translate into difference in aerodynamic force history, either in thrust production (thrust coefficient) or in the force necessary to produce the motion (here called normal-force coefficient). Further, there is no discernable Reynolds number effect, as slow motions and fast motions produced the same normalized aerodynamic coefficients, provided that the motions are fast enough to force plate rotation all the way against its hinge limiter.

Closer examination of thrust and normal-force history shows that the aerodynamic response to the plate translational kinematics is not quasi-steady, as both thrust and normal force decay from an initial maximum once the plate attains its incidence angle limit. This decay is roughly linear, at least for the larger semi-stroke to chord ratios. Double-hinged plates appear to have no advantage either in thrust production or figure of merit, relative to single-element plates. This suggests that at this level of analysis, wing structural flexibility does not offer an aerodynamic advantage.

References

[1] Doman, D., Oppenheimer, M., and Sigthorsson, D. "Dynamics and Control of a Minimally Actuated Biomimetic Hypersonic Vehicle: Part 1 – Aerodynamic Model". AIAA 2009-6160.

[2] Wood, R.J. "The First Takeoff of a Biologically Inspired At-Scale Robotic Insect". *IEEE Transactions on Robotics*, Vol. 24, No. 2., pp. 341-347, 2007.

[3] Dickson, W. and Dickinson, M., "The Effect on Advance Ratio on the Aerodynamics of Revolving Wings", Journal of Experimental Biology, Vol. 207, pp. 4269-4281, 2004.
[4] Granlund, K., OL, M., Bernal, L. and Kast, S., "Experiments on Free-to-Pivot Hover Motions on Flat Plates", AIAA 2010-4456
[5] Lentink, D. and Dickinson, M. H., "Rotational Accelerations Stabilize Leading Edge Vortices on Revolving Fly Wings," Journal of Experimental Biology, Vol. 212, April 2009, pp. 2705–2719
[6] Jones, A. and Babinsky, H., "Unsteady Lift Generation on Rotating Wings at Low Reynolds Numbers", Journal of Aircraft, Vol. 47, No. 3, 2010, pp. 1013–1021
[7] DeVoria, A., Mahajan, P. and Ringuette, M., "Vortex Formation and Saturation for Low-Aspect-Ratio Rotating Flat Plates at Low Reynolds Number", AIAA 2011-396
[8] Jones, A. and Babinsky, H., "Leading Edge Vortex Development on a Waving Wing at Reynolds Numbers Between 10,000 and 60,000", AIAA 2011-393
[9] Wan, H., Dong, H. and Huang, G., "Computational Fluid-Body interaction of Hinge Connected Flapping Plate in Hover" AIAA 2011-379
[10] Ol, M., Bernal, L., Kang, C.-K., and Shyy, W. "Shallow and Deep Dynamic Stall for Flapping Low Reynolds Number Airfoils". *Experiments in Fluids*, Vol. 46, Issue 5, pp. 883-901, May 2009.
[11] Ol, M., McAuliffe, B. R., Hanff, E. S., Scholz, U., Kaehler, Ch., "Comparison of Laminar Separation Bubble Measurements on a Low Reynolds Number Airfoil in Three Facilities", AIAA 2005-5149.
[12] Ol, M.V. "Vortical Structures in High Frequency Pitch and Plunge at Low Reynolds Number". AIAA-2007-4233.
[13] Eldredge, J. D., Toomey, J. and Medina, A., "On the Roles of Chord-Wise Flexibility in a Flapping Wing with Hovering Kinematics", *Journal of Fluid Mechanics*, Vol. 659, pp. 94-115, Sept. 2010
[14] Shyy, W. Aono, H., Chimakurthi, S.K., Trizila, P., Kang, C.-K., Cesnik, C.E.S., and Liu, H. "Recent Progress in Flapping Wing Aerodynamics and Aeroelasticity". *Prog. Aero. Sci.*, Vol. 43, No. 7, pp. 284-327, 2010.
[15] McCormick, B., Aerodynamics, Aeronautics and Flight Mechanics 2nd ed., Wiley 1995